Applied Microscopy
Korean Society of Microscopy
pISSN 2287-5123 · eISSN 2287-4445
http://dx.doi.org/10.9729/AM.2013.43.3.127

Crystallization Behavior of Al-Ni-Y Amorphous Alloys

Min Young Na, Kang Cheol Kim, Won Tae Kim[1], Do Hyang Kim*

Center for Non-crystalline Materials, Department of Materials Science and Engineering, Yonsei University, Seoul 120-749, Korea
[1]Department of Optical Engineering, Cheongju University, Cheongju 360-764, Korea

*Correspondence to:
Kim DH,
Tel: +82-2-2123-4255
Fax: +82-2-312-8281
E-mail: dohkim@yonsei.ac.kr

Received September 24, 2013
Revised September 25, 2013
Accepted September 25, 2013

The crystallization behavior in the $Al_{87}Ni_3Y_{10}$ and $Al_{88}Ni_3Y_9$ amorphous alloys has been investigated. As-quenched $Al_{87}Ni_3Y_{10}$ amorphous phase decomposes by simultaneous formation of Al and intermetallic phase at the first crystallization step, while as-quenched $Al_{88}Ni_3Y_9$ amorphous phase decomposes by forming Al nanocrystals in the amorphous matrix. The density of Al nanocrystals is extremely high and the size distribution is homogeneous. Such a microstructure can result from rapid explosion of the nucleation event in the amorphous matrix or growth of the preexisting nuclei embedded in the as-quenched amorphous matrix. The final equilibrium crystalline phases and their distribution at 873 K are exactly same in both $Al_{87}Ni_3Y_{10}$ and $Al_{88}Ni_3Y_9$ alloys.

Key Words: Amorphous alloy, Crystallization

INTRODUCTION

Recently, amorphous alloys attract much attention since they exhibit exotic properties due to their random atomic structure. Among the amorphous alloys, Al-based amorphous alloys are known to exhibit a good combination of mechanical and physical properties such as good ductility, high tensile strength, superior corrosion resistance, etc. which are superior to conventional Al-based alloys (Inoue et al., 1988). In particular, Al-transition metal (TM)-rare earth element (RE) alloys with a nanocomposite structure where Al nanocrystals are embedded in the amorphous matrix are known to exhibit a superior combination of tensile strength and ductility (Inoue, 1998). The most convenient way for obtaining such a nanocomposite structure in Al-based alloys is to partially devitrify the as-melt-quenched amorphous precursor. During partial devitrification of the amorphous precursor, it is essential that Al nanocrystals form as a product of the first crystallization stage. Al nanocrystals can from by primary nucleation event during heating of the as-melt-quenched amorphous phase or by growth of the preexisting quenched-in nuclei embedded in the amorphous precursor (Allen et al., 1998). However, many previous studies show that the amorphous precursor in Al-based alloys devitrifies in many different ways depending on the alloy system. Apart from the formation of Al nanocrystals, the first crystallization reaction Al-based amorphous alloys occurs by polymorphic crystallization forming intermetallic phase(s) or simultaneous crystallization forming Al and intermetallic phase (Battezzati et al., 2004). The simultaneous formation of Al and intermetallic phase can result from the eutectic reaction (Sahoo et al., 2005). Since partial devitrification of the Al-TM-RE amorphous alloys has been reported to produce high density of Al nanocrystals as well as different intermetallic phases embedded in the amorphous matrix, it is necessary to understand the crystallization behavior depending on the alloy chemistry and composition of the Al-TM-RE amorphous alloys. Therefore, the aim of the present study is to investigate the crystallization behavior in the Al-Ni-Y amorphous alloy. We show that even very small composition difference ($Al_{87}Ni_3Y_{10}$ and $Al_{88}Ni_3Y_9$, in at. %) can lead to different crystallization path in the Al-Ni-Y alloy system.

MATERIALS AND METHODS

Alloy ingots with a nominal composition of $Al_{87}Ni_3Y_{10}$ and

This work was supported by the Global Research Laboratory Program of the Korean Ministry of Education, Science and Technology.

$Al_{88}Ni_3Y_9$ were prepared by arc-melting in a water-cooled copper crucible under a protective argon atmosphere. The alloy was re-melted and then rapidly solidified into ~35 μm thickness ribbon-type samples by using a melt-spinning method. X-ray diffraction (XRD, D8 Discover; Bruker, Billerica, MA, USA) using monochromatic Cu Kα radiation was performed for structural characterization. Phase and microstructure analyses were done by transmission electron microscopy (TEM, Tecnai G2 F20; FEI, Hillsboro, OR, USA) combined with energy dispersive x-ray spectrometry (PV9761 Si(Li) detector; EDAX, Mahwah, NJ, USA). Thin foils for TEM investigation were prepared by a conventional ion milling method with acceleration voltage: 2.5 keV, current: 6 mA and Ar beam incident angle: 4~8°), and the specimen holder was cooled by liquid nitrogen during ion milling (Precision Ion Polishing System, PIPS 691; Gatan, Pleasanton, CA, USA). Thermal properties were measured using differential scanning calorimetery (DSC, DSC 7; Perkin Elmer, Waltham, MA, USA) at a constant heating rate of 0.67 K/s under a flow of purified argon.

RESULTS AND DISCUSSION

Fig. 1 shows DSC curves obtained from the as-melt-spun $Al_{87}Ni_3Y_{10}$ and $Al_{88}Ni_3Y_9$ alloy ribbons. The $Al_{87}Ni_3Y_{10}$ sample exhibits a clear glass transition, while the $Al_{88}Ni_3Y_9$ sample does not. Both samples exhibit three or four exothermic heat flow events due to crystallization of the glassy phase. The glass transition temperature (T_g) and the crystallization onset temperature (T_x) are marked by arrows on the DSC curves. For the $Al_{87}Ni_3Y_{10}$ sample, T_g, T_{x1}, T_{x2} and T_{x3} are 517 K, 541 K, 647 K and 692 K, respectively. The exothermic heat release due to crystallization, ΔH_1, ΔH_2, and ΔH_3 are 89 J/g, 51 J/g and 7 J/g, respectively. For the $Al_{88}Ni_3Y_9$ sample, T_{x1}, T_{x2}, T_{x3} and T_{x4} are 486 K, 595 K, 633 K and 699 K, respectively. The corresponding heat release, ΔH_1, ΔH_2, ΔH_3, ΔH_4 are 33 J/g, 39 J/g, 36 J/g and 9 J/g, respectively. The most striking differences between two DSC curves are: 1) the glass transition clearly occurs in the $Al_{87}Ni_3Y_{10}$ sample, but does not in the $Al_{88}Ni_3Y_9$ sample; and 2) the first crystallization peak in the $Al_{87}Ni_3Y_{10}$ sample is very sharp releasing larger amount of heat, but that in the $Al_{88}Ni_3Y_9$ sample is shallow releasing much smaller heat. To investigate the microstructural changes at each crystallization step, the $Al_{87}Ni_3Y_{10}$ ribbon sample was heated up to 544 K (first crystallization step) and 648 K (second crystallization step) in the DSC, and then cooled to room temperature. For the same purpose, the $Al_{88}Ni_3Y_9$ ribbon sample was heated up to 534 K (first crystallization step), 598 K (second crystallization step) and 642 K (third crystallization step). To confirm the stable crystalline phases, the both samples were heated up to 873 K far above the temperature range for the crystallization events. Fig. 2A and B shows XRD traces obtained from the $Al_{87}Ni_3Y_{10}$ and $Al_{88}Ni_3Y_9$ samples heated up to temperatures mentioned above. For the $Al_{87}Ni_3Y_{10}$ sample, the first crystallization event (544 K) produces Al and metastable phase. The XRD pattern indicates that the crystallization of the amorphous precursor is almost completed after the first crystallization step. The second crystallization event (648 K) occurs in the almost same way producing Al and metastable phase. But the metastable phase after the second crystallization event is different from that appeared after the first crystallization event. The peaks of metastable phases appearing after the first and the second crystallization steps could not be indexed unanimously in the present study. The XRD pattern obtained form the sample heated up to 873 K clearly reveals the appearance of the stable crystalline phases, Al, Al_3Y and $Al_{23}Ni_6Y_4$. However, the crystallization of the amorphous precursor in the $Al_{88}Ni_3Y_9$ sample proceeds in a completely different way, as can be seen in Fig. 2B. The first crystallization event (534 K) produces Al without any metastable phase. The XRD pattern indicates that large portion of the amorphous phase remains after the first crystallization step. The second crystallization event (598 K) occurs producing a metastable phase as well as Al, and comsumes remaining amorphous phase almost completely. The third crystallization event (642 K) occurs in the almost same way producing a metastable phase and Al. But, as in the case of the $Al_{87}Ni_3Y_{10}$ sample, the metastable phase after the thrid crystallization event is different from that appeared after the second crystallization event. Again, the peaks of metastable phases appearing after the second and the third crystallization steps could not be indexed unanimously in the present study. The XRD pattern obtained form the sample heated up to 873 K clearly reveals the appearance of the stable crystalline phases, Al, Al_3Y and $Al_{23}Ni_6Y_4$ which are exactly same as in the case of the $Al_{87}Ni_3Y_{10}$ sample. The XRD results shown in Fig. 2 indicate that the crystallization path is completely different

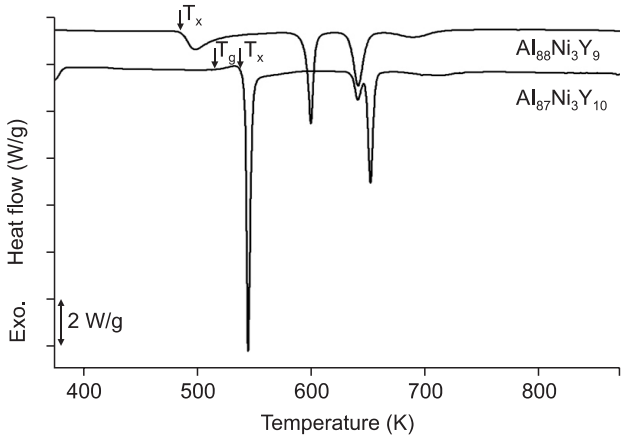

Fig. 1. Differential scanning calorimetery traces obtained from the as-melt-spun $Al_{87}Ni_3Y_{10}$ and $Al_{88}Ni_3Y_9$ alloy ribbons. T_x, the crystallization onset temperature; T_g, the glass transition temperature.

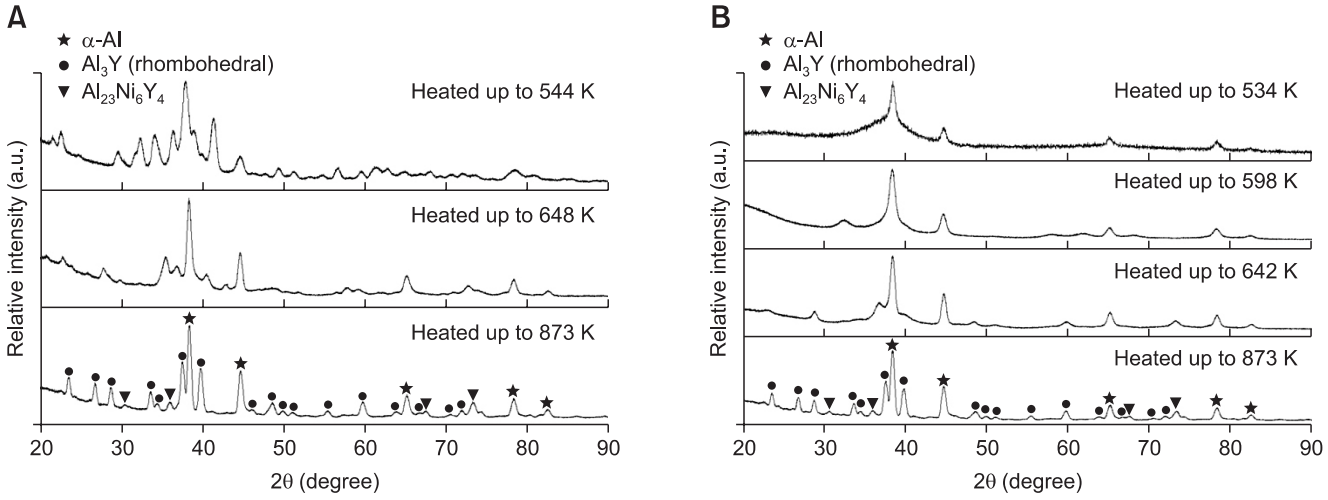

Fig. 2. X-ray diffraction traces obtained from $Al_{87}Ni_3Y_{10}$ alloy ribbon (A) and $Al_{88}Ni_3Y_9$ alloy ribbon (B).

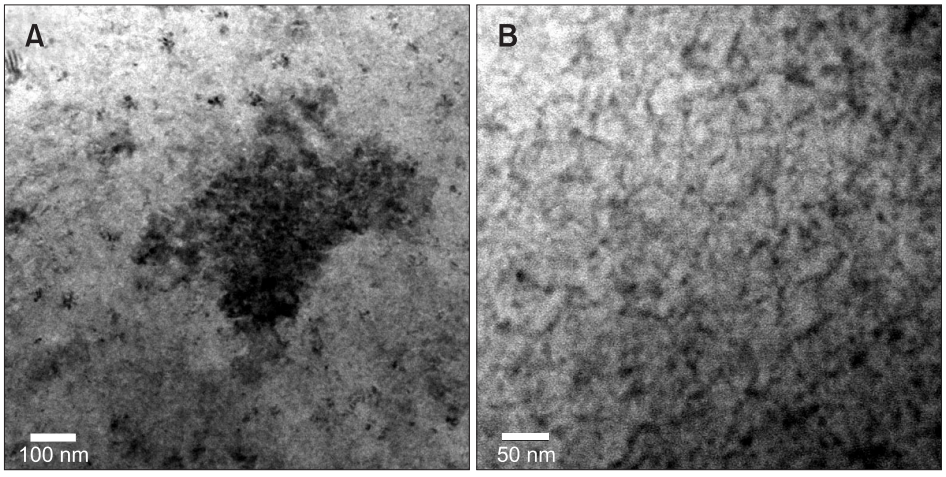

Fig. 3. (A) Bright field transmission electron microscopy (TEM) image and (B) high-angle annular dark-field scanning TEM image obtained from $Al_{87}Ni_3Y_{10}$ alloy ribbon heated up to 544 K.

in two samples, although the final stable crystalline phases are exactly the same.

Fig. 3 shows bright field (BF) TEM image and high-angle annular dark-field scanning TEM (HAADF-STEM) image obtained from the $Al_{87}Ni_3Y_{10}$ ribbon sample heated up to 544 K. From the BF TEM image it can be noticed that the crystallization is almost completed. The contrast variation resulting from the local composition change shown in Fig. 3B indicates that the microstructure consisted of fine composite structure of Al and intermetallic phase, as shown in the XRD pattern (Fig. 2). Fig. 4A and B shows BF TEM images with lower and higher magnification, respectively, obtained from the $Al_{88}Ni_3Y_9$ ribbon sample heated up to 534 K. As indicated in the XRD pattern in Fig. 2, ~20 nm size nanocrystals are uniformly distributed in the amorphous matrix. The corresponding selected area diffraction pattern (SADP) in Fig. 4C exhibits spotty ring pattern from the fcc structure of Al superimposed on the halo rings from the amorphous structure of the matrix. High resolution (HR) TEM image in Fig. 4D reveals the lattice fringes from Al nanocrystal of which the fcc structure can be confirmed in the inserted Fourier transformed (FR) diffraction pattern ([110] one of the fcc structure). It can be noticed that the density of the Al nanocrystals is extremely high and the size distribution is homogeneous. Such a microstructure can result from rapid explosition of the nucleation event (homogeneous nucleation) in the amorphous matrix or growth of the preexisting nuclei (quenched-in nuclei) embedded in the as-quenched amorphous matrix. Although more detailed analysis is required to verify the mechanism for the formation of high density Al crystals at the early stage of crystallization behavior in the $Al_{88}Ni_3Y_9$ ribbon sample, some previous studies inidcates that high density of quenched-in nuclei often exists in the as-quenched Al-based amorphous phase. The present result indicates that the state of the amorphous precursor is critically important in the early stage

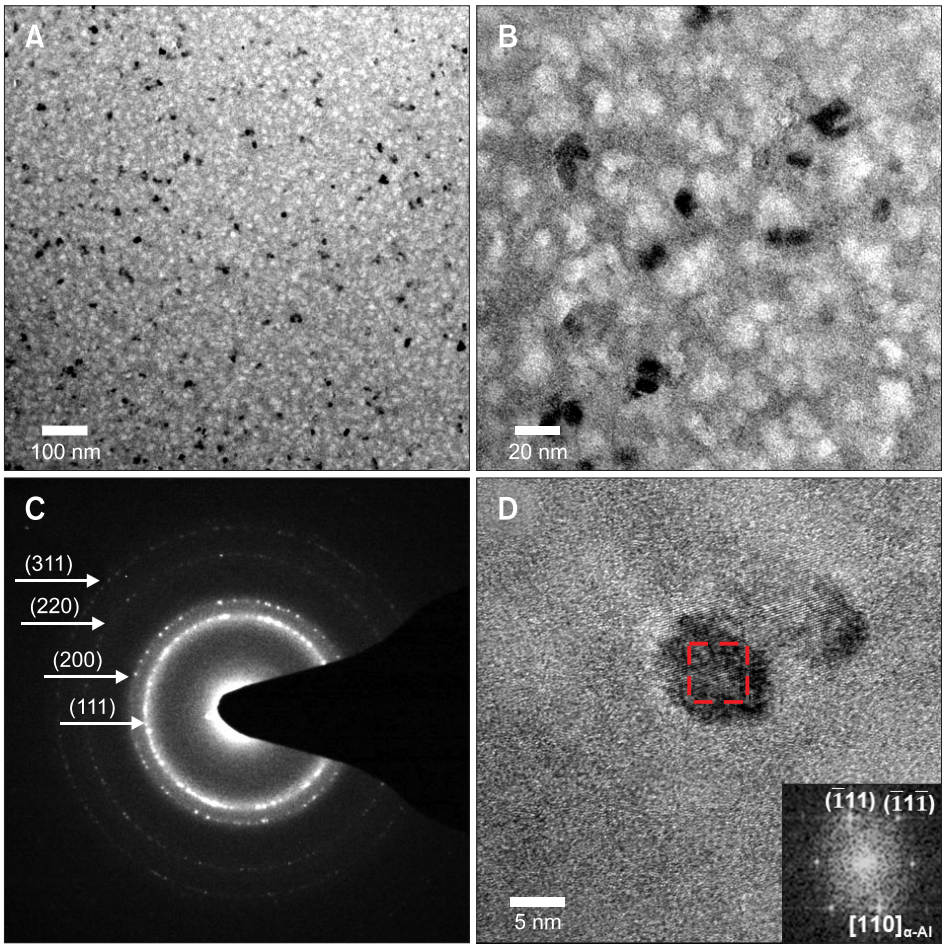

Fig. 4. Bright field transmission electron microscopy (BF TEM) images with (A) lower and (B) higher magnification, respectively, obtained from $Al_{88}Ni_3Y_9$ alloy ribbon heated up to 534 K. (C) Selected area diffraction pattern obtained from BF TEM image in (B). (D) High resolution electron microscopy image showing lattice fringes from Al nanocrystal with Fourier transformed diffraction pattern inserted.

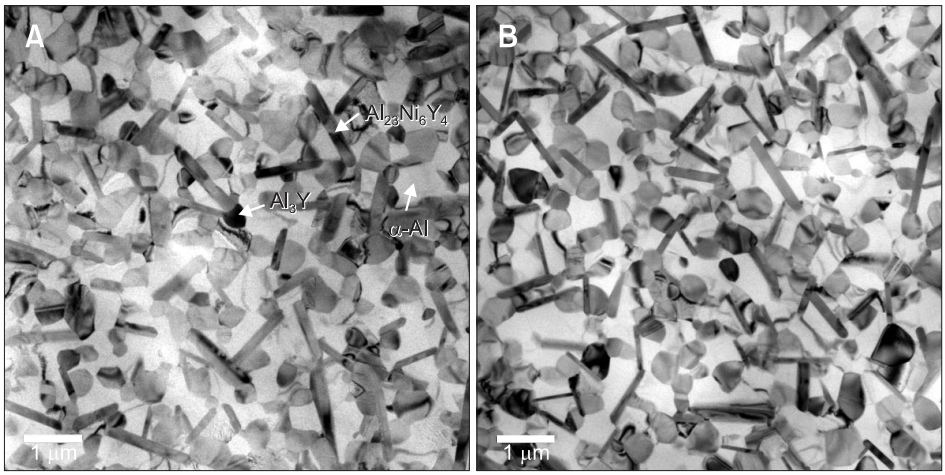

Fig. 5. Bright field transmission electron microscopy images obtained from (A) $Al_{87}Ni_3Y_{10}$ alloy ribbon and (B) $Al_{88}Ni_3Y_9$ alloy ribbon, respectively, heated up to 873 K.

crystallization behavior of Al-TM-RE amorphous alloys. BF TEM images in Fig. 5 compares the stable crystalline phases obtained from the $Al_{87}Ni_3Y_{10}$ and $Al_{88}Ni_3Y_9$ alloy ribbons, respectively, heated up to 873 K. It can be clearly noticed that the same crystalline phases (rod type $Al_{23}Ni_6Y_4$ and blocky type Al_3Y) are embedded in the Al matrix in both samples. Moreover, it can be noticed that their density and size distribution are also almost the same. The TEM results in Figs. 3-5 clearly indicate that the early stage crystallization behavior in the $Al_{87}Ni_3Y_{10}$ and $Al_{88}Ni_3Y_9$ amorphous alloys is completely different, although the final stable crystalline phases are exactly the same.

CONCLUSIONS

The present study shows that a small composition difference in Al-Ni-Y amorphous alloys can result in complete different early stage crystallization behavior, although the final equilibrium crystalline phases are the same. As-quenched $Al_{87}Ni_3Y_{10}$ amorphous phase decomposes by simultaneous formation of Al and intermetallic phase at the first crystallization step, while as-quenched $Al_{88}Ni_3Y_9$ amorphous phase decomposes by forming Al nanocrystals in the amorphous matrix. The density of Al nanocrystals is extremely high and the size distribution is homogeneous. Such a microstructure can result from rapid explosion of the nucleation event in the amorphous matrix or growth of the preexisting nuclei embedded in the as-quenched amorphous matrix. The result indicates that the state of the amorphous precursor is critically important in phase selection at the the early stage crystallization behavior in Al-TM-RE amorphous alloys. Interestingly, the final equilibrium crystalline phases (Al, Al_3Y and $Al_{23}Ni_6Y_4$) and their distribution at 873 K are exactly the same in both $Al_{87}Ni_3Y_{10}$ and $Al_{88}Ni_3Y_9$ alloys.

REFERENCES

Allen D, Foley J, and Perepezko J (1998) Nanocrystal development during primary crystallization of amorphous alloys. *Acta Mater*. **46**, 431-440.

Battezzati L, Kusy M, Rizzi P, and Ronto V (2004) Devitrification of Al-Ni-Rare earth amorphous alloys. *J. Mater. Sci*. **39**, 3927-3934.

Inoue A (1998) Amorphous, nanoquasicrystalline and nanocrystalline alloys in Al-based systems. *Prog. Mater. Sci*. **43**, 365-520.

Inoue A, Ohtera K, Tsai A-P, and Masumoto T (1988) Aluminum-based amorphous alloys with tensile strength above 980 MPa (100 kg/mm^2). *Jpn. J. Appl. Phys*. **27**, L479-L482.

Sahoo K, Wollgarten M, Kim K, and Banhart J (2005) Crystallization behavior and microhardness evolution in Al92-xNi8Lax amorphous alloys. *J. Mater. Res*. **20**, 2927-2933.